Shah *et al. Clin Trans Med (2018) 7:19*
https://doi.org/10.1186/s40169-018-0197-2

Clinical and Translational Medicine

RESEARCH

Open Access

Alk5/Runx1 signaling mediated by extracellular vesicles promotes vascular repair in acute respiratory distress syndrome

Trushil Shah[4], Shanshan Qin[1], Mona Vashi[1], Dan N. Predescu[1], Niranjan Jeganathan[1], Cristina Bardita[5], Balaji Ganesh[3], Salvatore diBartolo[1], Louis F. Fogg[2], Robert A. Balk[1] and Sanda A. Predescu[1*]

Abstract

Background: Pulmonary endothelial cells' (ECs) injury and apoptotic death are necessary and sufficient for the pathogenesis of the acute respiratory distress syndrome (ARDS), regardless of epithelial damage. Interaction of dysfunctional ECs with circulatory extracellular vesicles (EVs) holds therapeutic promise in ARDS. However, the presence in the blood of long-term ARDS survivors of EVs with a distinct phenotype compared to the EVs of non-surviving patients is not reported. With a multidisciplinary translational approach, we studied EVs from the blood of 33 patients with moderate-to-severe ARDS.

Results: The EVs were isolated from the blood of ARDS and control subjects. Immunoblotting and magnetic beads immunoisolation complemented by standardized flow cytometry and nanoparticles tracking analyses identified in the ARDS patients a subset of EVs with mesenchymal stem cell (MSC) origin ($CD73^{+}CD105^{+}Cd34^{-}CD45^{-}$). These EVs have 4.7-fold greater counts compared to controls and comprise the transforming growth factor-beta receptor I (TβRI)/Alk5 and the Runx1 transcription factor. Time course analyses showed that the expression pattern of two Runx1 isoforms is critical for ARDS outcome: the p52 isoform shows a continuous expression, while the p66 is short-lived. A high ratio Runx1p66/p52 provided a survival advantage, regardless of age, sex, disease severity or length of stay in the intensive care unit. Moreover, the Runx1p66 isoform is transiently expressed by cultured human bone marrow-derived MSCs, it is released in the EVs recoverable from the conditioned media and stimulates the proliferation of lipopolysaccharide (LPS)-treated ECs. The findings are consistent with a causal effect of Runx1p66 expression on EC proliferation. Furthermore, morphological and functional assays showed that the EVs bearing the Runx1p66 enhanced junctional integrity of LPS-injured ECs and decreased lung histological severity in the LPS-treated mice.

Conclusions: The expression pattern of Runx1 isoforms might be a reliable circulatory biomarker of ARDS activity and a novel determinant of the molecular mechanism for lung vascular/tissue repair and recovery after severe injury.

Keywords: Acute respiratory distress syndrome, Circulatory extracellular vesicles, Runx1 isoforms, Alk5, Endothelial cell injury

*Correspondence: Sanda_Predescu@rush.edu
[1] Department of Internal Medicine, Pulmonary, Critical Care and Sleep Medicine, Rush University Medical Center, 1750W Harrison St. 1535 JS, Chicago, IL 60612, USA
Full list of author information is available at the end of the article

Background

Acute respiratory distress syndrome is characterized by a consistent, recognizable pattern of lung injury; it is a life-threatening inflammatory lung condition with no drug treatment and high mortality [1–3]. The extent of repair mechanisms and outcome are very variable, and patients react differently to similar injury. If ARDS patients can survive the initial insult, lungs return to near-normal physiology except for a mild persistent reduction in diffusion capacity [4]. However, over the course of the disease, patients accumulate significant physical and cognitive disabilities [5]. Understanding the final common pathway of lung repair process might allow us to control the initial inflammation and regulate proliferation and fibrosis to achieve expedited recovery and thus, prevent the burden of physical and cognitive disabilities. Growing evidence suggests that intercellular communication of injured ECs with the EVs released in vitro by the cultured bone marrow-derived MSCs (EV_{MSC}) hold significant therapeutic promise for ARDS [6]. EVs are released from a variety of cells as byproducts of cell growth, apoptosis and in response to physiologic and pathophysiologic stimuli [7]. These EVs, also known as microparticles, microvesicles, microsomes, lipid vesicles and exosomes encapsulate small portions of the subjacent cytosol, creating a heterogeneous population of phospholipid-walled vesicles [7, 8]. The EVs circulate in the blood for an unknown length of time, interact with ECs and depending on their cellular origin/cargo may have different effects on EC function [8]. The studies using EVs released by the circulating MSCs in the blood are limited [9]. The number of circulating MSCs in peripheral blood is low, but injury and inflammatory states increase it; growing evidence indicates that MSCs migrate from their specific niches (i.e., bone marrow, adipose tissue, umbilical cord), transit through the blood to the injured tissue and promote the repair process [7, 9–11].

Recently we have shown that in vivo deficiency of intersectin-1s [(ITSN); a prevalent protein of the lung tissue] triggers apoptosis of mouse lung ECs, increase in the alveolar-capillary permeability, protein-rich edema and lung injury [12]. Moreover, the cells of the vascular system release in the systemic circulation of ITSN-deficient mice a population of EVs comprising the widely expressed TβRI/Alk5. These EVs interact with the dysfunctional lung ECs, mediate the intercellular transfer of Alk5 and rescue them from apoptotic death by activation of Erk1/2 MAPK pro-survival signaling. Within 2 weeks after severe injury, lung function returned to a normal state with little evidence of prior damage, suggesting that a lung repair process was critical for the remarkable recovery [12].

Thus, we hypothesized that similar to mouse studies, ARDS patients have a subset of circulatory EVs which rescue pulmonary microvascular ECs from apoptotic death. With a multidisciplinary translational approach, we studied EVs from the blood of ARDS patients and identified a sub-population whose phenotype is different from the EVs of non-surviving patients; due to their disease-specific cargo, they provide a survival advantage to ARDS patients.

Methods

Human lung microvascular ECs were obtained from Lonza (Walkersville, Inc., MD). The human bone marrow-derived MSCs, passage 1, were from the Institute for Regenerative Medicine, Texas A&M Health Science Center (Temple, TX).

Specific antibodies (Abs) were as follows: Alk5 rabbit Ab (Abcam; Cambridge, MA); ITSN-1 (Bethyl Laboratories, Inc., Montgomery, TX); actin and Prestige ITSN-1 Abs (Sigma-Aldrich; St. Louis, MO); TGFβRII, Runx1, Ki67, CD45, CD34, CD9, CD81, CD63, syntenin-1, mitofilin Abs (Santa Cruz Biotechnology; Santa Cruz, CA); CD31 Ab (Abbiotec, San Diego CA); phycoerythrin (PE)-conjugated CD62, CD61, CD14, CD68, CD144, CD73, CD105, CD45, CD34Abs, rabbit IgG-allophycocyanin (APC)-conjugated (Affymetrix; Santa Clara, CA) and biotin anti-human CD105 Abs (BioLegend; San Diego, CA); reporter Abs, fluorophor-conjugated, neutrAvidin-Alexa Fluor 594 and the Prolong Antifade reagent (Molecular Probes, Eugene, OR). All other reagents were purchased as follows: Spherotech nano fluorescent beads (Spherotech, Inc.; Lake Forest, IL); MagSiSta 1.0 magnetic beads (Amsbio LLC.; Cambridge MA); LPS from *Escherichia coli* 0111:B, the In Situ Cell Proliferation kit [Bromodeoxyuridine (BrdU) assay] and the protease inhibitor cocktail for mammalian cell and tissue extracts (Sigma-Aldrich; St. Louis, MO); 3-(4,5-dimethylthiazol-2-yl)-2,5-diphenyl tetrazolium bromide (MTT) Cell Proliferation Assay kit (ATCC; Manassas, VA); the bicinchoninic acid (BCA) Protein Assay Kit (Pierce; Rockford, IL).

Research subjects

Data and sample collection was done following the Rush University Medical Center (RUMC) Institutional Review Board (IRB), using an approved protocol (IRB# 14030705-IRB01) for investigational use of un-used diseased blood samples, drawn for routine medical care. Blood was collected from 33 patients admitted to RUMC ICU; all patients included, 18 years and older, were identified within 24 h of diagnosis and met moderate-to-severe ARDS criteria per "The Berlin Definition of ARDS" [13]. Age < 18 years, patients with isolated left heart failure and active malignancy and patients who

received immunosuppressant or chemotherapy during ARDS hospitalization were excluded. Age, sex, race, Acute Physiology and Chronic Health Evaluation II (APACHE II), Simplified Acute Physiology Score II (SAPS II), Sequential Organ Failure Assessment (SOFA) score, Lung Injury Score (LIS), P/F (PaO_2/FiO_2) ratio on the day of ARDS diagnosis, cause of ARDS, ventilator-free days, extracorporeal membrane oxygenation (ECMO), and length of stay were collected. Mortality from all causes was recorded at day 100. A detailed clinical data set is included in Additional file 1: Table S1.

Pathological slides (paraffin-embedded lung tissue) of five ARDS subjects and three non-disease controls (ND-Ctrl) identified from autopsy files were provided by the Department of Pathology, RUMC. Frozen lung tissue, normal and ARDS, was obtained from the National Disease Research Interchange. Clinical diagnosis, underlying conditions, and other pertinent clinical and laboratory data were reviewed.

Animals

CD1 male mice, 6–8 weeks old, 20–25 g weight, from Jackson Laboratory (Bar Harbor, ME), kept under standardized housing and feeding conditions were used. All mouse studies were approved and performed under the guidelines of RUMC Institutional Animal Care and Use Committee. The experiments were done under anesthesia [ketamine (60 mg/kg), acepromazine (2.5 mg/kg) and xylazine (2.5 mg/kg)] in 0.1–0.2 ml phosphate buffered saline (PBS)]. Three to five mice per experimental condition (wt-mice, LPS- and LPS ± EVs-treated mice) were used; all experiments were repeated at least three times. No mouse mortality occurred during the study.

Lung histology, immunohistochemistry (IHC) and morphometric analysis

Mouse lungs were inflated with 1% low-melting-point agarose in 10% formalin at a constant pressure of 25 cm H_2O, allowing for homogenous expansion of lung parenchyma, and then fixed in 4% paraformaldehyde for 48 h and paraffin-embedded [12]. Thin sections (4–5 μm), cut longitudinally, were stained with hematoxylin/eosin (H&E). Images were acquired with a 20× lens using a Zeiss AxioImager M1 motorized upright microscope equipped with AxioCam ICc1 R3 RGB color digital camera (Carl Zeiss MicroImaging, Inc., Thornwood, NY). Quantification of perivascular cuffing area was performed on small and medium-sized (20 μm ≥ diameter ≤ 100 μm) blood vessels using the NIH ImageJ software version 1.8.0_112 as described previously [14]. A minimum of 25 vessels per section was used (three sections/mouse, 3–5 mice/experimental condition). All experiments were performed at least three times with reproducible results.

IHC on paraffin-embedded human lung tissue sections was performed using the Prestige ITSN-1 Ab (C-terminal epitope; the only commercially available Ab efficient in IHC), CD31 Ab and Ki67 Abs. All were followed by the appropriate Alexa Fluor 488- or Alexa Fluor 594-conjugated reporters as previously described [12]. CD31 and Ki67 Abs were used at 1:200 dilution in 0.1% BSA in PBS, whereas ITSN-1 and was used at 1:100 dilution.

EVs isolation and standardization

EVs were isolated from the blood of ARDS patients (EV_{ARDS}) and control healthy subjects (EV_{Ctrl}). Whole blood was subjected to a first centrifugation [1.5×*g*; (3000 rpm) for 15 min, at 4 °C; Eppendorf microfuge, 5702R], to obtain the platelet-free plasma, that was then subjected to ultracentrifugation (Beckman Coulter, Optima™ MAX-XP, TLA-55 fixed angle rotor, 45-degree angle) at 79,700×*g*; (36,000 rpm), for 2 h, at 4 °C [15]. The EVs pellet was washed (3 × 10 min) in sterile PBS, subjected to ultracentrifugation as above and resuspended in 200 μl sterile PBS. To minimize potential changes, if any, in EVs' stability, only freshly prepared EVs were used for functional and morphological studies. EVs stored in liquid N_2 were used only for biochemical studies. To achieve high scientific rigor regarding reproducibility, the EVs were standardized according to the guidelines established by the International Society of Extracellular Vesicles for EVs isolation and analyses [16, 17]. We performed the following: (i) use of plasma for EVs retrieval; (ii) venipuncture and 0.109 M Na citrate as coagulant; (iii) room temperature (RT) for blood storage before first centrifugation; (iv) EVs isolation within 2 h of blood collection; (v) ultracentrifugation and immunobead magnetic separation for EVs isolation/enrichment, (vi) flow cytometry and calibrated/counted beads to establish the EVs' cellular origin and counts, (vii) collection of blood at the same time of the circadian day. Other key standardization factors specific to this study are: (i) constant blood volume to isolate EVs, (ii) constant 200 μl PBS to resuspend the EVs pellet, (iii) establish the Runx1p66/p52 ratio in the EVs isolated from the blood samples collected in week 2 of ICU stay (days 7–14), when the patients are in the subacute, proliferative phase of the disease, characterized by repair of the damaged alveoli and restoration of the barrier function [18].

ECs culture, LPS treatment, and EVs exposure

ECs, passages 3–5, were grown in Endothelial Basal Medium-2 and medium 199-supplemented with 20% fetal bovine serum (FBS) as previously described [19]. To mimic the inflammatory EC dysfunction, the ECs were

treated with 1 μg/ml LPS for 6 h (EC_{LPS}). Following LPS treatment, EC_{LPS} were exposed to three doses of EVs for 30 h, with 1 μg/ml LPS still present in the growth media.

Human MSCs culture and isolation of EV_{MSC}

Cells were used for the experimental protocols between passages 2 and 4. The MSCs were cultured in α-Minimum Essential Medium without ribonucleosides and deoxyribonucleosides containing 2 mM L-glutamine, 10% FBS (Atlanta Biochemicals, Inc., Flowery Branch, GA), 100 units/ml penicillin and 100 mg/ml streptomycin (Thermo Fisher Scientific, Hanover Park IL), in a humidified incubator at 5% CO_2 and 37 °C under sterile conditions [20, 21].

EV_{MSC} were obtained from the conditioned medium of MSCs at different time points of culture. MSCs were incubated for 24 h in medium depleted of FBS-derived EVs [22]. The conditioned was centrifuged at 1.5×*g*; (3000 rpm), for 15 min to remove cellular debris, then at 79,700 × g; (28,000 rpm), Beckman Coulter XL-90 ultracentrifuge, 70 Ti rotor, for 2 h at 4 °C. EV_{MSC} pellet was washed in PBS and subjected to a second ultracentrifugation. The EV_{MSC} were resuspended in sterile PBS according to the count of MSCs, usually 500 μl sterile PBS for 2×10^6 cells. EV_{MSC} were lysed for 1 h, at 4 °C in 50 mM Tris–HCl, pH 8.0, 150 mM NaCl, 1% NP-40 and protease inhibitor cocktail, used as per manufacturer's instructions. The protein content of the EV_{MSC} was quantified by the BCA assay with bovine serum albumin as standard.

Cell proliferation assays

BrdU assay

Cells were grown on coverslips for 48 h. BrdU incorporation was performed as described previously [12, 23]. Briefly, cells were incubated in culture medium containing 10 μM BrdU Labeling Solution for 6 h at 37 °C. Cells were then washed with PBS, fixed and the DNA denatured followed by incubation with BrdU-FLUOS Ab (45 min, 37 °C) in a humid chamber. Cells were again washed with PBS and the coverslips were mounted using the Prolong Antifade kit. The BrdU positive cells were counted on high power field images, and data were expressed as the number of BrdU positive cells per 50 high power fields.

MTT assay

Triplicate aliquots of ECs (10^6 cells suspended in 100 μl complete EC medium) were seeded onto a 96-well plate, and serial dilutions were prepared in EC medium. Cells, cultured for 48 h, were subjected to the LPS and EVs exposure as described above, followed by addition of 10 μl MTT Reagent to each sample. After 5 h incubation, 100 μl of detergent was added to each well; the plate was covered and kept in the dark at RT overnight. Absorbance was measured at 595 nm (OD^{595}) in a microtiter plate reader on the following day. Parallel triplicate experiments using non-treated ECs were performed, cells were counted using a hemocytometer, and a growth curve was generated to relate the OD^{595} values to the cell number per well [24].

Protein extraction and Western blot (WB) analyses

EV_{ARDS} and EV_{Ctrl} were lysed, and protein concentration was determined as described for EV_{MSC}. EVs lysates (individual samples) were analyzed for Alk5, TβRII and Runx1 protein content by WB via Alk5 (1:500), TβRII (1:500), Runx-1, CD9, CD81, CD63, syntenin-1, mitofilin (1:1000) Abs followed by the appropriate horseradish peroxidase-conjugated reporters [15]. WB analyses of EV_{ARDS} and EV_{Ctrl} lysates were normalized to equivalent μl blood or the total protein, as specified in the text. Actin cannot be used as loading control, as there is no evidence that EVs contain actin.

Flow cytometry and EVs counting

Total number/percentages of EVs were determined by standardized flow cytometry (Beckman Coulter Gallios flow cytometer with Kaluza G software for acquisition and Kaluza1.3 for analysis; [15, 25]), where the number of EVs was correlated to a fixed number of counting beads. EVs gating was accomplished by preliminary standardization experiments using Spherotech nano fluorescent size standard beads. Data are presented as dot plot and histograms and the results of data analysis as average % of total gated events (at least 10,000 events/sample) ± SEM. Percentage labeled EVs was determined by comparing with unstained control EVs, with gates set to exclude beads, background as determined by a buffer alone sample, as well as aggregates. Isotype-matched Abs served as control.

Nanoparticle tracking analysis (NTA)

The size distribution and concentrations of EV_{Ctrl} and EV_{ARDS} preparations were determined by NTA [26, 27], using a NanoSight NS 300 instrument (Malvern Instruments Limited; Malvern, Worcestershire, UK) and statistical analysis was performed for particles with diameter lower than 300 nm. Aliquots of each EV_{Ctrl} and EV_{ARDS} sample were diluted 1:100 in sterile PBS and placed in 1 ml syringes. Five 60 s frames were captured for each sample to ensure accurate quantitation of the sizes and

number of EVs. The data were averaged to determine the distribution and concentration of particles in each sample using the Nanosight NTA software Version 3.2 Dev Build 3.2.16.

Immunobead magnetic separation

Immunobead magnetic separation of Alk5-positive EVs was achieved in three steps as follows: EV_{ARDS} were labeled with Alk5 polyclonal Ab [15]; then a biotin-conjugated IgG secondary Ab was used as a bridge to allow the binding of the MagSi-STA 1.0 magnetic silica beads to the EV_{ARDS}. All three steps were followed by successive washings in PBS followed by ultracentrifugation as above. Isolation of CD105-positive EVs was achieved via biotinylated Abs using a similar approach. Aliquots of EVs bound to the magnetic beads were analyzed by SDS PAGE and WB for Alk5, Runx1, CD105, CD34 and CD45 immunoreactivity. EV_{ARDS} preparations were normalized to the blood volume used for isolation. Incubations of the EVs with the biotin-conjugated IgG secondary Ab and the MagSi-STA 1.0 magnetic silica beads by omitting the first Ab were used for controls.

EVs imaging

EVs were labeled with biotin/neutrAvidin–Alexa Fluor 594 or double labeled with Alk5 rabbit Ab/anti-rabbit IgG Alexa Fluor 488 and biotin/neutrAvidin–Alexa Fluor 594 reporters [15]. Final pellets were resuspended in PBS and fixed in 1% paraformaldehyde; aliquots were mounted on glass slides with Prolong Antifade Reagent. Isotype-matched IgG was used as a control. EVs were examined and photographed using a Zeiss AxioImager M1 microscope.

Power and statistical analysis

The human analysis used a Kaplan–Meier test (SPSS software, Version 22), to determine if the survival is longer among the Runx1p66 immunoreactive subjects. An effect size of d = 1.20 was obtained [28], which may be a little optimistic. Thus, assuming a more conservative effect of d = 0.80 (Cohen's estimation of a 'large' effect), for our sample size of 29 ARDS patients (four patients out of the total of 33, were used only for flow cytometry; no Runx1 expression pattern was analyzed), a one-tailed alpha of 0.05, a power of 0.97 are obtained.

A standard heterogeneous *t* test was used to compare data between groups.

To look for differences in the two groups as shown in Table 3, we used χ^2 test for differences in mortality and sex and utilized student *t* test to look for differences in age, P/F ratios, APACHE II, SAPS II, SOFA score, and LIS.

Results

Human ARDS lung tissue is deficient of ITSN and shows limited EC proliferation

As chronic deficiency of ITSN in a murine model of acute lung injury (ALI)/ARDS triggers a repair process characterized by EC proliferation and vascular remodeling [12], we investigated whether ITSN deficiency is a feature of ARDS human lung tissue. ITSN/CD31 IHC was used to study the cellular distribution of ITSN in the lung tissue of ARDS and ND-Ctrl specimens. ITSN/Alexa Fluor 594 staining is limited in the ARDS specimen (55 years old, male; pneumonia; Fig. 1a, inset, arrows). The typical ARDS morphology with tissue congestion, inflammatory infiltrates, and edema (Fig. 1a, arrowheads) is noticeable. The ND-Ctrl shows significant ITSN immunoreactivity and co-localization with the EC marker CD31 (Fig. 1b, inset). For biochemical evaluation of ITSN expression, total protein was extracted from frozen human ND-Ctrl lung (62 years old male, myocardial infarction) and ARDS tissue (36 years old male, pneumonia),

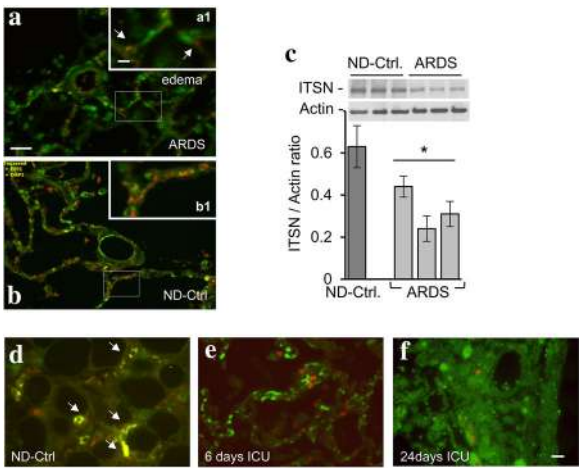

Fig. 1 Human ARDS lung tissue is deficient of ITSN and shows limited EC proliferation. **a**, **b** Representative ITSN-Alexa Fluor 594/CD31-Alexa Fluor 488 IHC of lung sections of ARDS and ND-Ctrl specimens, respectively; insets are higher magnifications of boxed areas. The arrowheads in **a** indicate a lung vessel with perivascular edema. Arrows in **a**, inset indicate the limited co-localization ITSN/CD31. Bars: 60 µm (**a**, **b**); 100 µm (insets). **c** Total protein extracted from ND-Ctrl and ARDS frozen lung tissues was analyzed by SDS PAGE (50 µg/lane) and WB with ITSN Ab. Actin served as loading control. The graph in **c** shows the average of ITSN/Actin ratio ± SD as determined by densitometric analyses of representative blots. *$p < 0.01$ vs. ND-Ctrl. n = 3. **d** Representative Ki67-Alexa Fluor 594/CD31-Alexa Fluor 488 IHC of lung sections of ND-Ctrl, and 2 ARDS specimens, a 55 year old male (**e**), and a 65 year old male (**f**); the number of days in ICU are indicated. Arrows in **d** indicate the co-localization CD31/Ki67. Sepsis was the cause of ARDS. Five ARDS and three ND-Ctrl samples were analyzed. Bar: 50 µm. n = 3 experiments

from three different locations. WB followed by densitometry indicate that expression of ITSN protein is decreased 40–70% in ARDS samples compared to ND-Ctrl (Fig. 1c). This finding is highly relevant to ECs of the lung, as ECs represent about 50% of the lung tissue [29].

As ECs proliferation and increased microvascular density were critical for the repair process of murine lung injury [12], we next used lung autopsy slides of 5 ARDS patients who survived 6–24 days in ICU and subjected them to dual Ki67 (proliferation marker)/CD31 IHC to investigate the extent of EC proliferation. ARDS specimens show limited ECs proliferation (Fig. 1e, f), most likely the cause of the poor lung architecture and increased fibrosis in these patients. Ki67/CD31 co-localization on a lung section of a ND-Ctrl specimen is shown for comparison (Fig. 1d, arrows).

The systemic circulation of ARDS patients contains elevated levels of EV_{ARDS} immunoreactive to TβRI/Alk5

EV_{ARDS} and EV_{Ctrl} were isolated from the blood of ARDS and control subjects within less than 2 h of blood withdrawal. Accurate data for EVs concentration were obtained by standardized flow cytometry [25]. EVs' count indicated mean values of 13,680 EV_{ARDS}/1 µl blood and 8615 EV_{Ctrl}/1 µl blood, Fig. 2a. The EVs were also quantified by comparing the total protein amounts in the EV_{ARDS} and EV_{Ctrl} pellets. The protein content of EV_{ARDS} is ~2-fold higher compared to the EV_{Ctrl}, Fig. 2b, an expected higher ratio given the aggregates content, excluded from the gated flow cytometry count. This ratio was recorded regardless of the timing of blood collection from all ARDS patients studied, consistent with reports of elevated levels of circulating EVs in disease settings [9, 11, 30]. As ARDS lung tissue is deficient of ITSN, we investigated whether EV_{ARDS} contain the

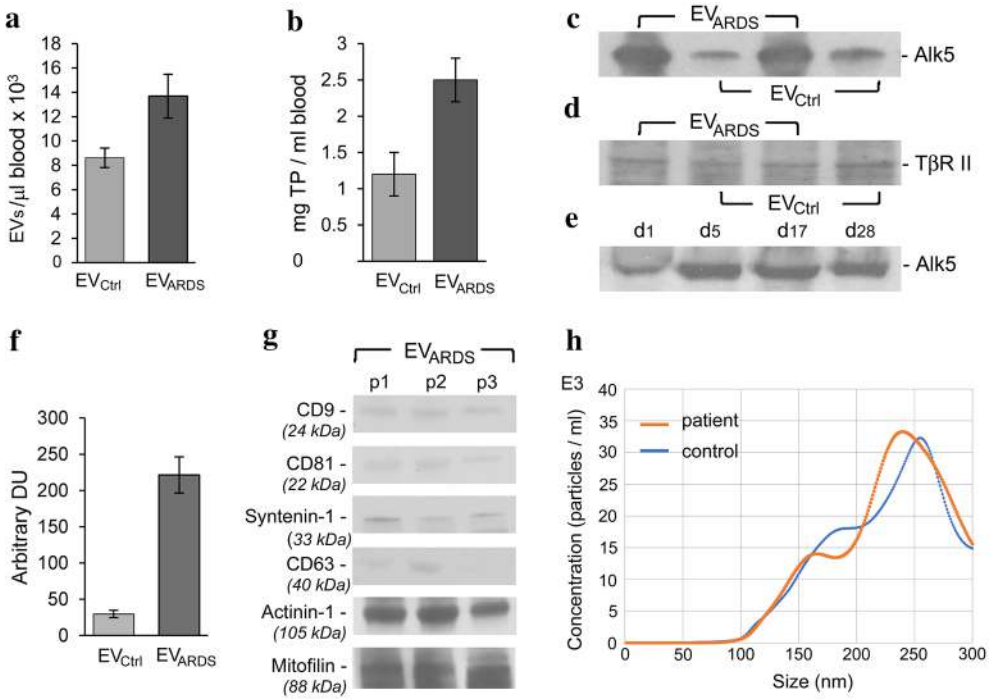

Fig. 2 ARDS subjects show increased counts of circulatory EV_{ARDS} immunoreactive to TβRI/Alk5. **a** The mean count for EVs isolated from the blood of the ARDS patients (EV_{ARDS}) was 13,680 ± 1811, with a range 11,000–17,500; Nine EV_{ARDS} preparations from nine different ARDS patients were used. The EV_{Ctrl} mean count indicated 8615 ± 768, with a range 7700–9200; three preparations from the blood of three different control subjects were used. Data are normalized per 1 µl blood. Three independent experiments were performed. **b** Amount of total protein in the EV_{ARDS} pellet and EV_{Ctrl} pellet, normalized to 1 ml blood. Data are plotted as mean ± SD; *$p < 0.05$ vs. controls. **c**, **d** WB of Alk5 and TβRII protein expression in two EV_{ARDS} and two EV_{Ctrl} lysates, normalized to equivalent µl blood; n = 9. Actin cannot be used as loading control, as there is no evidence that the EVs contain actin. **e** Time course analysis of Alk5 in EV_{ARDS} in one of the above ARDS cases; n = 3. Day 1 is first day in ICU. **f** Densitometric analysis of Alk5 protein expression in the $EV_{Ctrl\ and}$ EV_{ARDS} lysates. Data are plotted as mean ± SD; *$p < 0.05$ vs. controls. **g** Size distribution and concentration of exosomes and smaller than 300 nm diameter microparticles in the isolated EV_{Ctrl} and EV_{ARDS} preparations, measured by NTA; n = 3. **h** Representative WB analyses of EV_{ARDS} fractions of three different patients using Abs specific for CD9, CD81, syntenin-1, CD63, actinin-1 and mitofilin. Actinin-1 and mitofilin, considered specific markers for the non-exosomal microvesicles are enriched in the EV_{ARDS} preparations; n = 3

TβRI/Alk5, similar to the EVs released in the circulation of ITSN-deficient mice. EV_{ARDS} and EV_{Ctrl} lysates were analyzed for their Alk5 content by WB, Fig. 2c. Alk5 was found in both EV_{Ctrl} and EV_{ARDS}. However, as indicated by densitometric analyses of representative blots, Fig. 2f, Alk5 expression was sevenfold greater in EV_{ARDS} compared to EV_{Ctrl}, suggestive of a greater expression of Alk5 in EV_{ARDS} compared to the EV_{Ctrl}. Since TβRI signals through a heteromeric TβRI/TβRII complex and since the EVs of ITSN-deficient mice were immunoreactive for the TβRII [15], we also analyzed the EV_{ARDS} for their TβRII content by WB. EV_{ARDS} were immunoreactive to the TβRII Ab, Fig. 2d, suggesting that the human EVs, bear the Alk5/TβRII heteromers. Furthermore, time course analyses of Alk5 protein expression in the EV_{ARDS} from different ARDS subjects at several time points of ICU stay indicate no significant changes in Alk5 from day 5 to day 28 of ICU stay, Fig. 2e, the time interval used to collect blood and isolate EV_{ARDS}.

As the size ranges of EVs, from exosomes (diameter 40–120 nm) to microparticles, diameter 200–1000 nm [31], cannot be considered absolute and given the unfeasibility to isolate a pure microparticle fraction, exclusively [16], we also evaluated the exosomal content by NTA approach (Fig. 2g). No discernible peak was detected for particle sizes of 40–120 nm. We also evaluated the purity of the isolated EVs fractions by WB analyses using specific Abs against CD9, CD81, syntenin-1 and CD63, reported to be enriched in exosomes, and actinin-1 and mitofilin enriched in non-exosomal EVs populations [22]. As shown in Fig. 2h, the EVs fractions of three different ARDS patients showed scarcely detectable immunoreactivity for exosomal markers and strong immunoreactivity for the non-exosomal EVs, consistent with an enriched non-exosomal fraction of EV_{ARDS}. Thus, the isolation procedure applied indicates that the exosome and microparticle fractions are distinct in both size and biochemical makeup.

It is widely accepted that it is difficult to distinguish between two subpopulations of EVs based only on the size and protein composition [22]. Since a precise definition for exosomes and microparticles remains to be resolved, we refer to the population of membrane vesicles isolated according to our experimental protocol (79,700 × g, 2 h), as EVs.

EV_{ARDS}Alk5 sub-population is derived from the MSCs

Labeling of EV_{ARDS} using allophycocyanin-Alk5, phycoerythrin- and pacific blue-conjugated cell surface markers, followed by flow cytometry analyses of the mean values/percentages recorded, indicate: (i) a high content (> 50%) of EV_{ARDS} immunoreactive to Alk5 Ab, (ii) immunoreactivity of EV_{ARDS}Alk5 to CD105 and CD73 Abs, suggestive of MSC-origin, (iii) 4.7-fold increase in the count of EV_{ARDS} of MSC-origin compared to EV_{Ctrl}, as determined by tri-color labeling of EVs (Table 1). For data analysis, scatter and fluorescence noise was determined by running double filtered buffer alone, and a gate was drawn over the background noise to exclude those events (Fig. 3a, Gate A). Representative forward (FS) and side scatter (SS) plot for unstained EV_{ARDS} and background fluorescence in PE and APC channels for the unstained samples are shown as dot plot (b) and individual histograms (c, d). Samples of isolated EVs (Gate D) and 2 µm beads (Gate B) were run, to determine approximate sizing of the EVs relative to the beads as well as to determine background fluorescence (Fig. 3e, i). The majority of EVs were found to be around 1 µm in size (Gate D). Next, EV_{ARDS} stained with Alk5-APC/CD105-PE Abs were analyzed by flow cytometry to evaluate the co-expression of Alk5 and CD105 on the EV_{ARDS} (Fig. 3e, Gate D). A representative plot of double stained EV_{ARDS} (Fig. 3f) and the individual histograms for PE-CD105 (Fig. 3g) and APC-Alk5 (Fig. 3h) are shown. Similarly, EV_{ARDS} co-stained with Alk5-APC/CD73-PE Abs were analyzed by flow cytometry to evaluate the co-expression of Alk5 and CD73 on the EV_{ARDS} (Fig. 3i, Gate D). A representative flow cytometry plot of Alk5-APC/CD73-PE-labelled EV_{ARDS} is shown in Fig. 3j. The individual histograms for CD73-PE (Fig. 3k) and Alk5-APC (Fig. 3l) are shown.

MSCs origin of EV_{ARDS} was also confirmed by no detectable immunoreactivity to the hematopoietic markers CD45/CD34 [32], as shown by magnetic bead immunoisolation of CD105-positive EV_{ARDS} followed by WB (Fig. 3m). As the cellular origin of EVs is a defining factor for the magnitude of the physiological effect elicited [33],

Table 1 A subset of EV_{ARDS} has mesenchymal stem cell (MSC)-origin and shows significant increase in the ARDS subjects compared to controls

Variable (EVs/µl)	Mean		Fold increase
	EV_{Ctrl}	EV_{ARDS}	
Alk5	3446 (40%)	7200 (53%)	2.1
Alk5/CD73	53 (0.6%)	294 (2.1%)	5.6
Alk5/CD105	478 (5.5%)	1008 (7.4%)	2.1
Alk5/CD62	632 (7.3%)	1021 (7.5%)	1.6
Alk5/CD68	534 (6.2%)	1123 (8.2%)	2.1
Alk5/CD31	432 (5.0%)	782 (5.7%)	1.8
Alk5/CD73/CD105	49 (0.57%)	234 (1.7%)	4.8

Mean numbers/percentages of EV_{Ctrl} and EV_{ARDS} co-labeled with allophycocyanin (APC)-Alk5, phycoerythrin (PE) and pacific blue-conjugated cell surface markers. We used CD62 for platelets [59], CD68 as monocytes/macrophage markers [60, 61], CD31 for ECs [62, 63] and CD73 and CD105 for MSCs [32]. Isotype matched Abs served as control; n = 7 EVs isolates/experimental condition, in three independent experiments

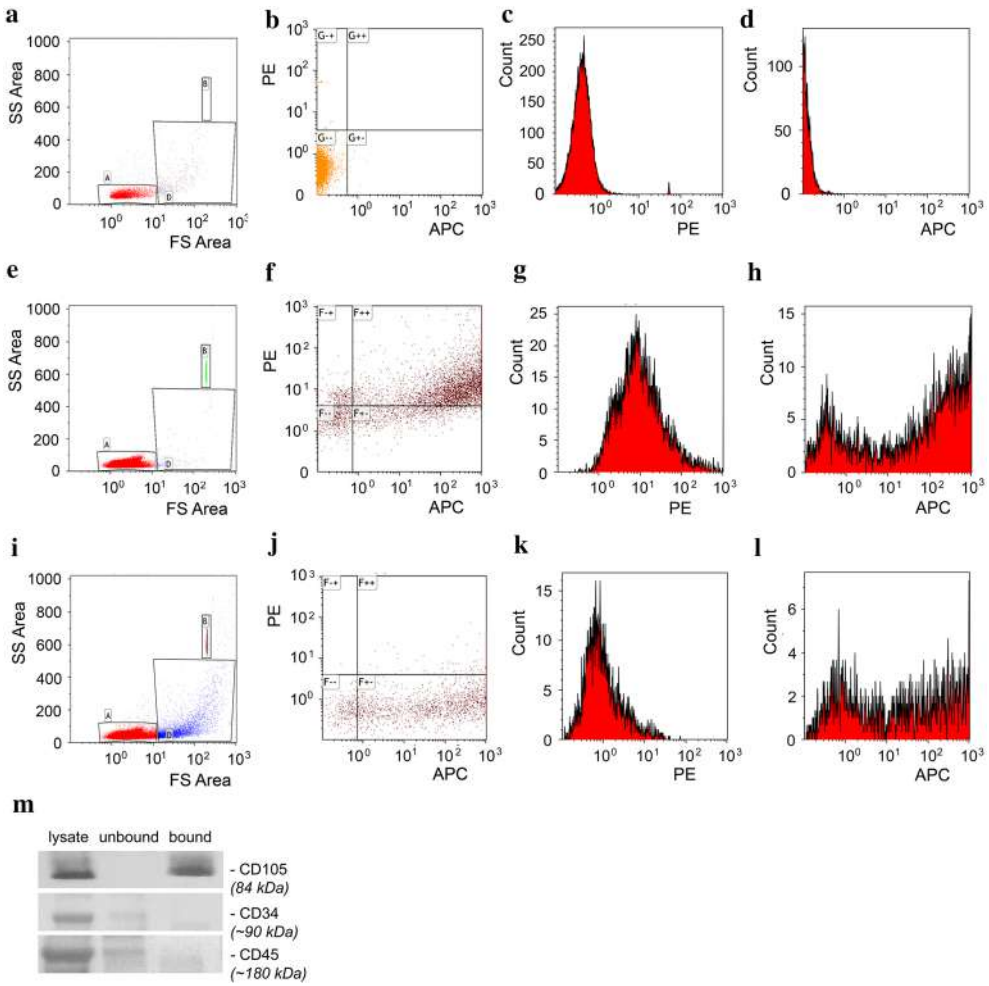

Fig. 3 EV_{ARDS}Alk5 sub-population is derived from the MSCs. Unstained EVs were used as controls to determine fluorescence background as well as for gating purposes. **a** Representative forward and side scatter plot for unstained EVs. Background fluorescence in the PE and APC channels for the unstained samples shown as dot plot (**b**) and individual histograms (**c**, **d**). Similar, representative plot of EVs stained with Alk5-APC/CD105-PE Abs (**f**) to analyze the co-expression of these markers on the EV_{ARDS} (**e**, Gate D), together with the individual histograms for CD105-PE (**g**) and Alk5-APC (**h**). Representative plot of EVs stained with Alk5-APC/CD73-PE Abs (**j**) to analyze the co-expression of these markers on the EV_{ARDS} (**i**, Gate D), along with the histograms for CD73-PE (**k**) and Alk5-APC (**l**) are also shown. n = 9 EV_{ARDS} and 5 EV_{Ctrl} isolates. **m** Representative immunoisolation of $CD105^{+}$ EV_{ARDS} Alk5 via biotin-conjugated CD105 Ab and streptavidin magnetic beads incubation. Lysates of EV_{ARDS}, bound and unbound EV_{ARDS} fractions were analyzed by SDS PAGE and WB. No immunoreactivity to CD45 and CD34 is detected. n = 6 EVs isolates/experimental condition, in three independent experiments

and considering the 4.7-fold increase in the count of the EV_{ARDS} of MSC origin compared to controls, the most significant increase compared to the EV_{ARDS} of other cellular origins identified, we focused on this disease specific subset of EV_{ARDS}.

Runx1p66 isoform provides a survival benefit to ARDS patients

Given the involvement of Runx1 transcription factor in angiogenesis and MSCs proliferation [34] and our findings that lung tissue of non-surviving ARDS patients shows deficient EC proliferation, we investigated whether the EV_{ARDS} contain Runx1 by WB analysis. Two Runx1 isoforms were detected—a 52-kDa protein present in all EV_{ARDS} as well as in EV_{Ctrl}, and a less characterized 66-kDa isoform [35], present only in some EV_{ARDS} samples, Fig. 4a. This observation is of particular interest, as out of 29 samples analyzed, 20 samples show Runx1p66 immunoreactivity; 14 out of these 20 EV_{ARDS} samples also display a higher than 0.5 Runx1p66/p52 ratio and belong to ARDS patients still alive, Table 2. Three samples (S5, S14, S35) belong to ARDS patients that died

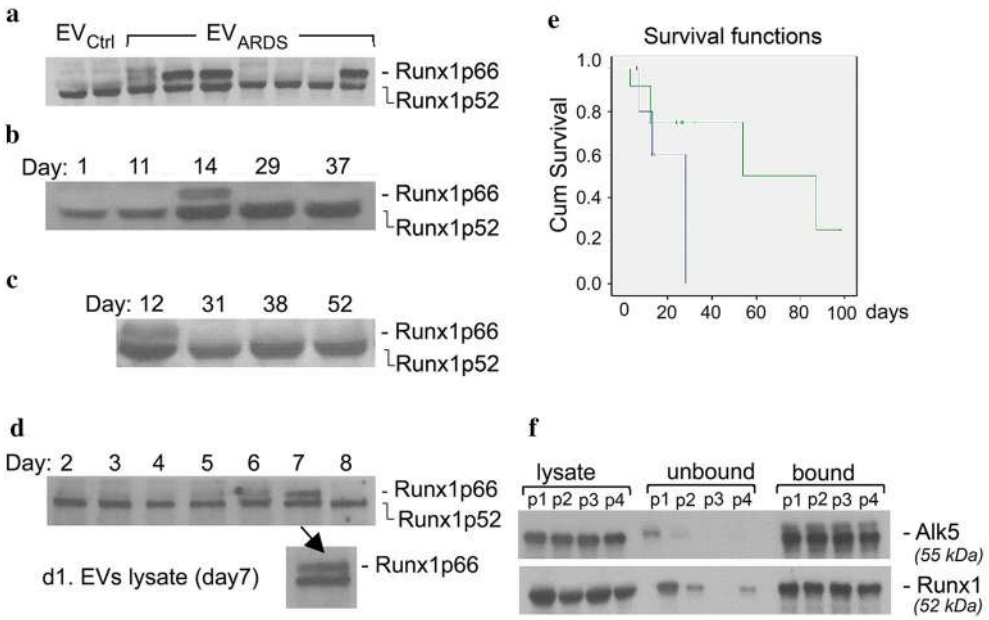

Fig. 4 Runx1p66 protein expression is short-lived and provides a survival advantage. **a** Representative Western blot of Runx1 protein expression in seven EV_{ARDS} and two EV_{Ctrl} preparations. Normalization was achieved to the volume of blood used (typically 1.5 ml) for EVs isolation. **b** Time course analysis of Runx1 in EV_{ARDS} of a long-term ARDS survivor (S6) and panel **c**, a non-surviving ARDS patient (S12). Expression of Runx1p52 gradually increases from day 1 to day 37 in ICU in the EV_{ARDS} of long-term survivor. Even if the number of blood samples available for later time points assessed was lower due to death of some patients, the time course analysis data are representative for at least three long-term survivors and three non-surviving ARDS patients. **d** Western blot of Runx1 expression in lysates of cultured human bone marrow-derived MSCs (d2–d8) as well as in lysates of the EV_{MSC} released at d7 (d1). 30 µg protein/lane; n = 3. **e** The Kaplan–Meier statistic shows the improved survival for the EV_{ARDS}Alk5Runx1p66 patients. Out of 33 ARDS patients included in the study, only 29 patients (multiple samples) were used to investigate the Runx1 isoform content and the Runxp66/p52 ratio. **f** Four EV_{ARDS} preparations (p1–p4; isolated from 1.8 ml of blood) were labeled with a biotinylated Alk5 rat Ab followed by streptavidin-conjugated magnetic beads. An isotype matched IgG for Alk5 was used as control. Aliquots of EV_{ARDS} lysates, unbound and bound fractions were analyzed by SDS PAGE and Western blot with Alk5 and Runx1 Abs. EV_{ARDS} are immunoreactive to Runx1p52 isoform only as the blood samples used belong to either non-surviving ARDS subjects or to surviving ARDS subjects, but collected in week 1 of ICU stay, when the EV_{ARDS} do not show Runx1p66 immunoreactivity. n = 9 different ARDS patients; Three independent experiments were performed

Table 2 Expression of Runx1 isoforms in EV_{ARDS} and ARDS outcome

ARDS sample	Runx1^{p66} expression	p66/p52 ratio	ICU length of stay (days	ARDS outcome
S2; S4; S5*; S6; S10; S13; S14*; S17; S18; S25; S26, S28; S31; S32; S33; S34; S35*;	Yes	High	28	14 long-term survivors 3 deceased*
S11; S12; S15	Yes	Low (< 0.5)	51	All deceased
S3; S9; S19; S23; S27;	No	–	12.4	All alive (the endogenous lung ability to repair is sufficient for recovery)
S7; S8; S20; S22	No	–	14.5	All deceased (the endogenous lung ability to repair not sufficient for recovery and no Runx1^{p66} expression)

29 EV_{ARDS} preparations and 3 EV_{Ctrl} were lysed and subjected to WB analyses with Runx1 Ab. Runx1 immunoreactivity was quantified by densitometry (NIH ImageJ) and used to establish the Runx1p66/p52 ratio. EV_{ARDS} samples S5*, S14* and S35* illustrate special situations of three ARDS patients that died despite their high Runx1p66/p52 ratio due to other complications (S5) or removal of life support at family's request (S14, S35)

despite a high Runx1p66/p52 ratio (> 0.5) due to special circumstances, as described in Table 2 (legend), while the remaining three samples (S11, S12, S15) have a low Runx1p66/p52 ratio (< 0.5) and also belong to non-surviving ARDS patients. Other 4 EV_{ARDS} samples (S7, S8, S20, and S22) with no Runx1p66 immunoreactivity

belong to non-surviving ARDS patients, as well. Notably, the last 5 EV_{ARDS} samples belong to long-term ARDS survivors that spent on average only 12.4 days in ICU; these EV_{ARDS} show no Runx1p66, Table 2, raising the possibility that the circulatory EV_{ARDS}Runx1p66 might be needed only when the endogenous lung MSCs [36, 37] and thus, the ability of lung tissue to repair, a hallmark of the normal course of recovery from ALI in some patients [38], are not sufficient. The ratio Runx1p66/p52 was established in all cases in EV_{ARDS} isolated from blood samples collected in week 2 of ICU stay, a key standardization factor for patients' disease stage. Histologically, days 7–14 are recognized as the sub-acute, proliferative ARDS phase, characterized by lung cell proliferation and attempts of repairing the damaged alveoli and restoration of the barrier function [18]. These observations strongly suggest that expression of Runx1p66 and a high Runx1p66/p52 ratio provide a survival benefit to ARDS patients. It seems that despite the heterogeneous etiology of ARDS and various treatment/medication received, concurrent illness, mechanical ventilation, active inflammation, etc., the transient expression of Runx1p66 and a high Runx1p66/p52 ratio are part of a common pathway of lung response leading to ARDS resolution.

We also performed a time course analyses of Runx1 expression in EV_{ARDS} of long-term ARDS survivors, Fig. 4b, and non-survivors, Fig. 4c; Runx1p52 is detected at each time point analyzed, while Runx1p66 is detected only at day 14 in ICU for the ARDS survivor, in the case shown. This transient expression of Runx1p66 was also detected in cultured human bone marrow-derived MSCs, Fig. 4d. Briefly, we analyzed cultures of human bone marrow-derived MSCs, passage 2–3, for their Runx1 expression, each day starting at about 5% confluence (day 2) and after the cultures had expanded to about 80% confluence (day 8). Runx1p52 was expressed starting at day 2 at each time point analyzed, while Runx1p66 was transiently expressed (days 6 and 7), and released in the EVs recovered from the growth medium.

We then analyzed the ARDS patients and their EV_{ARDS}′ Runx1p66 and p52 isoform content regarding to the severity of the disease, demographics and mortality, Table 3. Only 3/17 patients with a high ratio (>0.5) died as compared to 7/12 patients who had a low ratio (<0.5) or Runx1p66 negative. This difference in mortality was statistically significant by Chi square test ($\chi^2 = 5.15$, $p = 0.023$). The likelihood ratio is 5.218. Furthermore, we compared these two groups for differences in age, sex, SAPS II score, APACHE II score, SOFA score, LIS and P/F ratio at the onset of ARDS and ICU length of stay. None of these were statistically significant, but patients with high Runx1p66/p52 ratio tended to be younger (mean age 41.76 ± 6.9 vs. 50.25 ± 9.4). Despite the relatively small sample size of this study, there is no question that the survival/censoring times for participants with this Runx1p66 isoform was much larger than it was for those without it; the patients are censored as the total survival time cannot be accurately determined for all participants [39]. Combining mortality and censored times, the mean time for the Runx1p66 group is 32.10 days (sd = 24.35) while the mean time for the Runx1 p66-negative group was 12.89 days (sd = 6.37). A simple, heterogeneous t-test between the two groups is statistically significant ($t = 3.29$, $df = 23.90$, $p = 0.003$).

The differences between the two conditions are also clearly seen in a life table, Fig. 4e. While the Kaplan–Meier statistic for this table is not quite significant ($\chi^2 = 3.65$, $df = 1$, $p = 0.056$), it is also clear that the

Table 3 Comparison for baseline severity of disease, demographics and mortality between patients with Runx1p66/p52 high ratio vs. patients Runx1p66 negative or low Runx1p66/p52 ratio

	Runx1 p66/p52 high ratio	Low Runx1 p66/p52 ratio or p66 negative	p value
No.	17	12	–
Mortality	3 (17.6%)	7 (58.33)	0.023 (OR = 5.15)
Age	41.76 ± 6.4	50.25 ± 9.4	0.142
Sex	10F/7M	5F/7M	0.362
SAPS II	47.23 ± 6.9	53.33 ± 7.25	0.254
APACHE II	23 ± 3	25.5 ± 4.35	0.349
SOFA	10.94 ± 1.58	13.08 ± 2.18	0.124
Lung Injury Score	2.91 ± 0.33	3.09 ± 0.49	0.574
P/F ratio at onset of ARDS	118.13 ± 25.04	96.04 ± 19.21	0.213
ICU length of stay	28.76 ± 10.05	22.42 ± 13.66	0.460

APACHE II Acute Physiology and Chronic Health Evaluation II; *SAPS II* Simplified Acute Physiology Score II, *SOFA* Sequential Organ Failure Assessment score, *LIS* Lung Injury Score, *P/F* PaO_2/FiO_2 ratio on the day of diagnosis of ARDS; Values are mean ± SD

improved mortality for the Runx1p66 group begins at about 15 days, and then persists from then on. Another remarkable finding was that 100% of the high p66/p52 ratio sample was still alive at day 100 (not plotted), Additional file 1: Table S1. Thus, correlation of EV_{ARDS} immunoreactivity for Runx1 with survival data indicates that the transient expression of Runx1p66 and a high Runx1p66/p52 ratio provide a survival benefit to ARDS patients.

Alk5 and Runx1 reside on the same EV_{ARDS} population

We used magnetic separation of Alk5-positive EV_{ARDS} via MagSi-streptavidin beads to address whether Alk5 and Runx1 reside on the same EV_{ARDS} population. Briefly, Alk5-positive EV_{ARDS} were labeled with an anti-Alk5 goat Ab, followed by a biotinylated rabbit anti-goat IgG and MagSi-streptavidin beads. WB analyses of bound and unbound EV_{ARDS} indicated that all EV_{ARDS} immunoreactive to Alk5 possess Runx1 (Fig. 4f), suggesting that a significant sub-set of EV_{ARDS} comprises both Alk5/TβRI receptor and Runx1 transcription factor. However, a small fraction of Runx1-positive EV_{ARDS} does not contain Alk5, Fig. 4f (unbound fractions).

EV_{ARDS}Alk5Runx1p66 stimulate ECs proliferation

First, EV_{ARDS} were visualized by biotin/neutrAvidin–Alexa Fluor 594 labeling, as recently described by us for the EVs isolated from the blood of ITSN-deficient mice [15]. Similar to the mouse EVs, fluorescently labeled human EVs show a continuous, donut-shape (Fig. 5a,

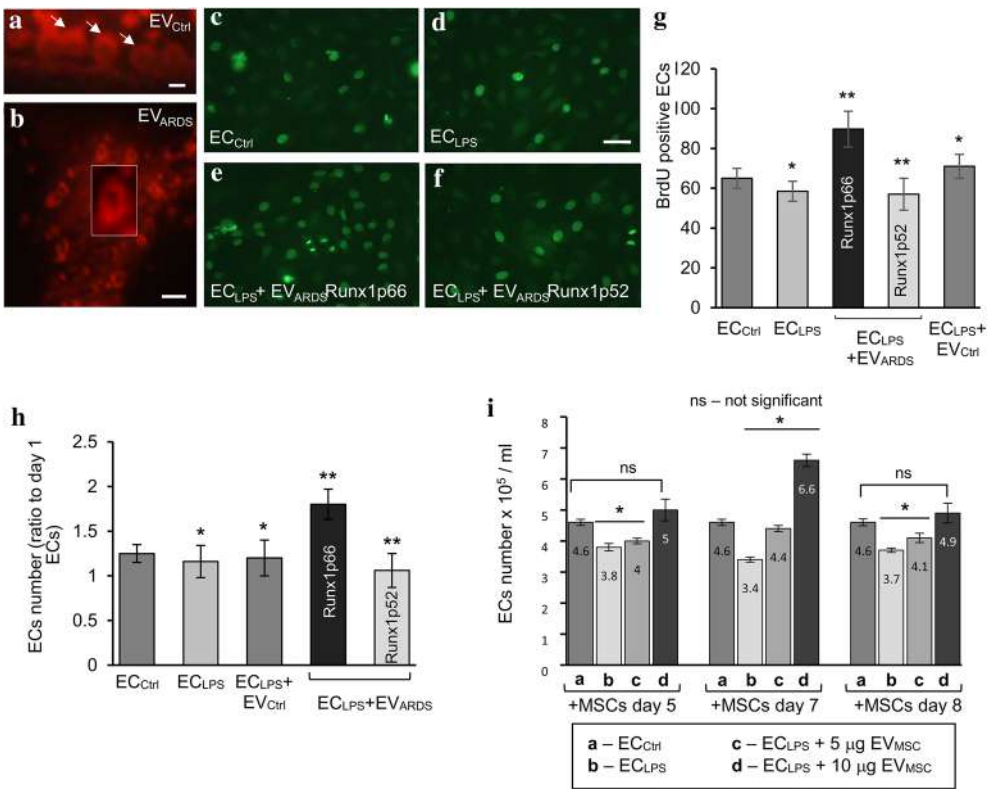

Fig. 5 EV_{ARDS}Alk5Runx1p66 increase proliferation of LPS-treated ECs. Biotin/neutrAvidin-Alexa Fluor 594 labeling of EVs isolated from a human healthy donor (**a**, EV_{Ctrl}) and an ARDS subject (**b**, inset; EV_{ARDS}). Arrows in **a** indicate several donut-shaped EV_{Ctrl}. Bars: 1 µm (**a**, and **b** inset), 2 µm (**b**). n = 3. BrdU labeling of EC_{Ctrl} (**c**), EC_{LPS} (**d**) and EC_{LPS} exposed to EV_{ARDS}Alk5Runx1p66 isolated from the blood of a long-term ARDS survivor (**e**) and EC_{LPS} exposed to EV_{ARDS}Alk5Runx1p52 isolated from the blood of a non-surviving ARDS patient (**f**). A dose of 1.6×10^3 EV_{ARDS}/1 ml growth medium was used for the micrographs shown. Bars: 50 µm (**c**–**f**). **g** Quantification of BrdU-positive cells. The results are expressed as BrdU-positive ECs/high power field (50 power field images/experimental condition). Data are representative of three different experiments and were normalized per total number of cells counted. Values are shown as mean ± SEM. n = 3; *p < 0.05; **p < 0.01. **h** MTT assay and cell counting of EC_{Ctrl} and EC_{LPS} exposed for 3 days to EV_{Ctrl} and EV_{ARDS}, as above (ratio 2:1 EV_{ARDS}:EV_{Ctrl}). Data are normalized to day 1 EC_{Ctrl}. Values are shown as mean ± SEM. n = 3; *p < 0.05; **p < 0.01. **I** EC_{Ctrl} (a bars), EC_{LPS} (b bars), EC_{LPS} + 5 µg EV_{MSC} (c bars) and EC_{LPS} + 10 µg EV_{MSC} (d bars) were counted 3 days post-EV_{MSC} exposure. Briefly, EV_{MSC} released by 3×10^6 MSCs, at day 5, day 7 and day 8, were resuspended in 50 µl sterile PBS; 1 dose of 10 µg/ml protein was found efficient in inducing proliferation of EC_{LPS}. All data labels are included for each bar. Values are shown as mean ± SEM. n = 3 experiments (triplicate wells each); *p < 0.01 vs. EC_{Ctrl}

arrows; b, inset). As human ARDS lung tissue is deficient in EC proliferation, we next evaluated the biological activity of EV_{ARDS} on cultured human lung ECs proliferation. To mimic the inflammatory EC dysfunction, the ECs were treated with 1 μg/ml LPS for 6 h (EC_{LPS}), and then exposed to three doses of EV_{ARDS}Alk5Runx1p66 or EV_{ARDS}Alk5Runx1p52 [0.8×10^3, 1.6×10^3 (the dose shown in Fig. 5e, f) and 3.2×10^3 per 1 ml growth medium] for 30 h, followed by BrdU cell proliferation assay [24]. ECs with no LPS and no EV_{ARDS} exposure (EC_{Ctrl}, Fig. 5c), EC_{LPS} (Fig. 5d) and EC_{LPS} exposed to EV_{Ctrl} at 2:1 (EV_{ARDS}:EV_{Ctrl}) ratio, according to the in vivo situation (not shown), were used for comparison. Morphometric analyses of the BrdU-positive ECs nuclei (Fig. 5g), indicated that 1 μg/ml LPS for 6 h minimally inhibits ECs proliferation (less than 10%). Exposure of EC_{LPS} to 1.6×10^3 EV_{ARDS}Alk5Runx1p66 caused about 38% increase in the BrdU-positive cells compared to EC_{LPS}. The EV_{ARDS}Alk5Runx1p52 did not induce EC_{LPS} proliferation, regardless of the dose used. Exposure of EC_{LPS} to EV_{Ctrl} (2:1 ratio EV_{ARDS};EV_{Ctrl}) increased the number of BrdU-positive cells less than 10%. The proliferative effects of EV_{ARDS}Alk5Runx1p66 at a lower or, the higher doses used were less evident. Furthermore, the MTT assay [24] to evaluate the effects of the EV_{ARDS} on LPS-injured ECs (Fig. 5h) biochemically, indicated that 1.6×10^3 EV_{ARDS}Alk5Runx1p66/1 ml growth medium at day 3 post-exposure, increase the number of EC_{LPS} by 44%, compared to EC_{Ctrl} (Fig. 5h). EC_{LPS} exposed to EV_{Ctrl} show similar proliferation as EC_{LPS}, both slightly lower than EC_{Ctrl}. EC_{LPS} exposed to 1.6×10^3 EV_{ARDS}Alk5Runx1p52/1 ml growth medium showed some variability in their proliferative effects depending on the EV_{ARDS} sample used; on average however, the EV_{ARDS}Alk5Runx1p52 slightly decreased, by less than 8%, the number of the BrdU-positive cells compared to EC_{LPS} (Fig. 5h). Based on these data, we concluded that the under inflammatory conditions, EV_{ARDS}Alk5 Runx1p66 stimulate ECs proliferation.

Runx1p66 accounts for EC proliferation

The proof-of-concept that Runx1p66 isoform accounts for EC proliferation was obtained when EC_{LPS} were exposed to EV_{MSC}, isolated from the conditioned media of cultured MSCs (passage 3–4), as described under Methods. EV_{MSC} were isolated at day 7, when Runx1p66 immunoreactivity is detected and at days 5 and 8, with no Runx1p66 is detected; two EV_{MSC} doses were used: 5 μg/ml (low dose) and 10 μg/ml (high dose). The quantitative assessment indicated that 10 μg/ml EV_{MSC} increased proliferation of EC_{LPS} at day 7 by 40%, compared to EC_{Ctrl}, Fig. 5I (bar d vs. bar a).

Minimal EC proliferation, with no statistical significance was noted at days 5 and 8, for the high EV_{MSC} dose. No EC proliferation was noticed for the low EV_{MSC} dose, regardless of Runx1p66 content; the finding is consistent with an EV_{MSC} basal threshold for inducing proliferation, as already reported by us [15] and with the beneficial effects of the high Runx1p52/p66 ratio. The data support the causal impact of Runx1p66 expression on EC proliferation.

EV_{ARDS}Alk5Runx1p66 improve the interendothelial junctional integrity of LPS-treated ECs

As the integrity of the interendothelial junctions (IEJs) is vital for barrier function and edema resolution, we investigated the biological activity of freshly isolated EV_{ARDS} in mitigating the LPS effects on IEJs. Cultured ECs treated with 1 μg/ml LPS for 6 h, as above followed by 30 h exposure to three doses (0.8×10^3, 1.6×10^3 and 3.2×10^3 per 1 ml growth medium) of EV_{ARDS}Alk5Runx1p66, were subjected to VE-cadherin Ab/Alexa Fluor488 immunocytochemistry. The integrity of IEJs in EC_{LPS} treated with 1.6×10^3 EV_{ARDS}Alk5Runx1p66 (Fig. 6d) was improved compared to EC_{LPS} with no EV_{ARDS}Alk5Runx1p66 exposure (Fig. 6b, c) or exposed to an equal dose of EV_{ARDS}Alk5Runx1p52 of a non-surviving ARDS patient (Fig. 6e). Figure 6a shows for comparison the IEJs in EC_{Ctrl}. Interendothelial gaps are significantly larger at 30 h post-LPS exposure without any EV_{ARDS} treatment (Fig. 6c) compared to 6 h LPS time point (Fig. 6b). Quantitative assessment of intercellular gaps (NIH ImageJ), shows that EV_{ARDS} bearing Runx1p66 reduced significantly, more than 60% the interendothelial gap area in LPS-treated ECs, while the EV_{ARDS} with no Runx1p66 by only 27%, Fig. 6f. The surface of the interendothelial gaps at 30 h post-LPS is 40% greater compared to 6 h LPS time point with no EV_{ARDS} exposure. The effects of the lower and the higher EV_{ARDS} doses were less noticeable.

EV_{ARDS}Alk5Runxp66 decrease lung histological severity in LPS-treated mice

Lung injury was induced in mice by intraperitoneal delivery of 3.5 mg/kg LPS (sub-lethal dose) as described in [6]; 8 h post-LPS treatment, mice were injected retro-orbitally with two EV_{ARDS} doses: 2.9×10^5 and 5.8×10^5 (dose shown in Fig. 7) in 100 μl sterile PBS. Assessment of lung pathology on H&E stained mouse lung sections, 48 h after EV_{ARDS}Alk5Runx1p66 administration shows reduction of inflammatory cells, decreased perivascular cuffing and less thickening of the interstitium (Fig. 7e) compared to LPS-only treated mice (Fig. 7b–d). Lung histological severity is not improved by EV_{ARDS}Alk5Runx1p52 (EV_{ARDS} of the same patient in week 1 in ICU, when no Runx1p66 immunoreactivity

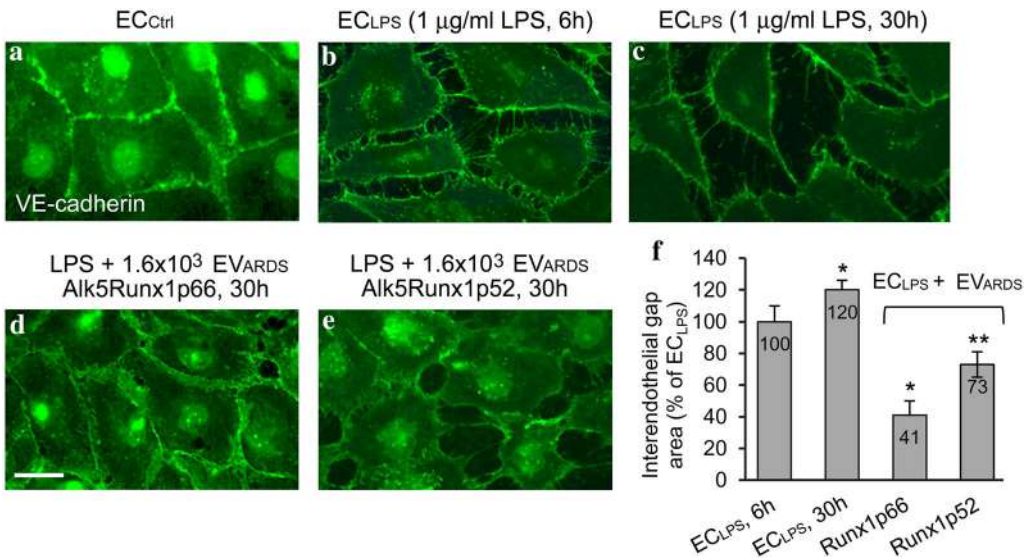

Fig. 6 EV_{ARDS}Alk5Runx1p66 improve the interendothelial junctional integrity of LPS-treated ECs. Representative VE-cadherin/Alexa Fluor 488 staining of EC_{Ctrl} (**a**), ECs treated with 1 µg/ml LPS (EC_{LPS}) for 6 h (**b**) and 30 h (**c**); EC_{LPS} (6 h) were treated for 30 h with either (**d**) 1.6×10^3 EV_{ARDS}Runx1p66/1 ml growth media or (**e**) 1.6×10^3 EV_{ARDS}Runx1p52/1 ml growth media (non-surviving ARDS patient). Bars: 15 µm (**a**–**e**). **f** Morphometric analysis of the interendothelial gap area. All data labels are included for each bar. n = 3 EVs preparations/experimental condition, in three independent experiments; *p < 0.01; p** < 0.05

is detected), Fig. 7f, or EV_{ARDS} a non-surviving patient (week 2 ICU), Fig. 7g. The 48 h time point post-EV_{ARDS} has been selected as mice need at least 72 h for recovery after sub-lethal LPS, with no other treatment [40]. The benefit of the low EV_{ARDS}Alk5Runx1p66 dose was less evident (not shown). The lung histology of mice treated with LPS only and mice treated with LPS followed by EV_{Ctrl} display no detectable differences at this time point (not shown). Mice injected with PBS served as controls (Fig. 7a). Quantitative assessment of perivascular cuffs, sign of a compromised endothelial barrier indicates ~60% reduction in EV_{ARDS}Alk5Runx1p66-treated mice, when the high dose has been used, compared to LPS-treated mice (Fig. 7h). The beneficial effects of the low EV_{ARDS}Alk5Runx1p66 dose were less visible (Fig. 7h). Mice treated with EV_{ARDS}Alk5Runx1p52, regardless of the source of the EV_{ARDS} preparation—non-surviving ARDS subjects or long-term survivors—show no decline in the perivascular cuffing (Fig. 7h). These data strongly suggest that despite the complex biochemical makeup of EV_{ARDS}, Runx1p66 contributes significantly to improve the junctional integrity and reduce perivascular cuffing of LPS-injured ECs.

Discussion

In the current study, we have identified in the blood of long-term ARDS survivors a subset of EV_{ARDS} with MSC origin and different phenotype compared to the circulatory EV_{ARDS} of non-surviving patients. To our knowledge, the presence in the blood of long-term ARDS survivors of a distinct population of circulatory EV_{ARDS} with MSC-origin and different biochemical makeup compared to the EV_{ARDS} of non-surviving patients has not been reported so far. Similar to our observations however, limited studies reported a protective role of leukocyte-derived EVs with an increased count in the blood and bronchoalveolar lavage of ARDS patients [41]. More recently, Shaver et al. [42], found a strong association between the lower levels of circulatory EVs and the development of ARDS in patients with sepsis. Nonetheless, the biochemical makeup or mechanism(s) involved remain unknown. We show now that a subset of the EV_{ARDS} with MSC origin and increased count comprises the widely expressed TβR1/Alk5 and the Runx1 transcription factor. The protein expression pattern of two Runx1 isoforms during the first month in the ICU appears critical for the ARDS outcome: the p52 isoform shows a continuous expression, while the p66 isoform is short-lived. Significantly, a high ratio Runx1p66/p52 was associated with survival. We have also found that this difference in the temporal expression pattern of Runx1 isoforms is a characteristic of cultured human bone marrow derived MSCs, as well, consistent with the recent similar reports for cells with non-hematopoietic lineage [43].

Previous studies have shown that the MSCs decrease the severity and even improve survival in various

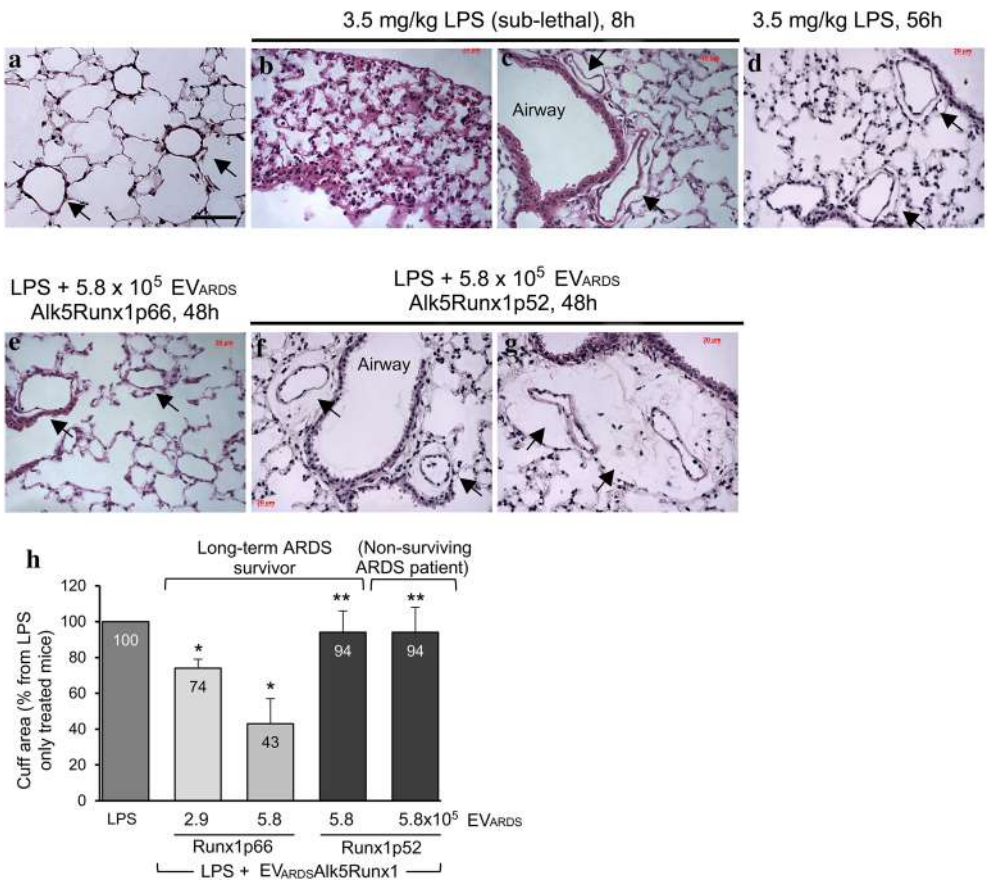

Fig. 7 EV_{ARDS}Alk5Runx1p66 decrease lung histological severity and restore lung endothelial permeability in LPS-treated mice. Representative H&E of lung sections illustrates the extent of perivascular cuffs (arrows) and thickening of the interstitium in mice treated with LPS only (**b**, **c**, **d**), EV_{ARDS}Alk5Runx1p66 (**e**), EV_{ARDS}Alk5Runx1p52 isolated from the blood of a long-term ARDS survivor, week 1 in ICU, when the EV_{ARDS} do not show Runx1p66 immunoreactivity (**f**) and EV_{ARDS}Alk5Runx1p52 of a non-surviving ARDS (**g**). **a** Comparison the H&E staining of a control, untreated mouse lung section. **h** Morphometric analyses of perivascular cuff area using the NIH ImageJ software; only small and medium-sized ($20 \geq$ diameter ≤ 100 µm) blood vessels were included. All data labels are included for each bar. Bar: 50 µm (**a**–**g**). n = 3 different EV_{ARDS} preparations in three independent experiments; *$p < 0.01$; **$p < 0.05$

animal models of ALI/ARDS [44–47]. MSCs produce a wide variety of molecules including hematopoietic and angiogenic factors as well as chemokines and generally, render their effects by immunomodulation [48]. Recently, Zhu and colleagues showed that MSC-derived EVs are therapeutically effective following *Escherichia coli* endotoxin-induced ALI [49], at least in part due to the expression of keratinocyte growth factor mRNA transferred to epithelium by these EVs. To date, no study has looked at the role of EV_{MSC} in endothelial recovery in ARDS. Loss of endothelial barrier function is one of the key events for the development of ARDS. It is both necessary and sufficient for the pathogenesis of ARDS regardless of epithelial damage [50, 51]. As shown by multiple studies, MSCs improve both endothelial and epithelial permeability and function [48]. Also, since every patient' response varies to similar injury (e.g. sepsis), the severity of ARDS as well as clinical course, vary. This variability can be in part played by the presence of endogenous MSCs and their mediators that are delivered to injured ECs by EVs.

Similar to the ITSN-deficient mouse studies, the subpopulation of human MSC-derived EV_{ARDS} are immunoreactive to both TβR1 and TβRII, a strong indication that these EV_{ARDS} are equipped with "ready-to-signal" TβR1/TβRII heteromeric complexes [52]. Our recent work demonstrated a functional relationship between the intercellular transfer of Alk5 by circulatory EVs and ECs proliferation via a novel molecular mechanism for TGFβ/Alk5-dependent Erk1/2 kinase signaling [15]. We have shown that ITSN deficiency leading to nonproductive assembly of the Alk5-Smad-SARA (Smad anchor for receptor activation, also known as ZFYVE9) signaling complex and preferential formation of the

Alk5–mSos–Grb2 complex accounts for Erk1/2 activation downstream of Alk5 and proliferation of pulmonary ECs. Thus, after the interaction of EV_{ARDS} with the injured, ITSN-deficient ECs, the TGF-β/Alk5 signaling switches from Smad2,3 to Erk1/2 MAPK pathway and downstream Cdk6 activation leading to the proliferation of ECs and microvascular remodeling [15, 53]. Runx1 is a target for both Cdk6 and Erk1/2 [35, 54], and it seems that in inflammatory settings associated with ARDS, the TGFβ/Alk5-dependent Erk1/2 kinase activation, Cdk6 regulation and Runx1 transcriptional activity are responsible for ARDS-associated microvascular remodeling and lung tissue repair.

Runx1, a member of runt-related transcription factors, is critically necessary for angiogenesis, T-cell and B-cell maturation [55, 56] and regulation of the cell cycle [56]. It has been reported that Runx1 plays a critical role in the mouse lung inflammation following LPS-induced injury [57]. Increased respiratory distress, inflammation, and pro-inflammatory cytokine were observed in the Runx1-deleted mice after pulmonary LPS exposure; Runx1 deletion was associated with the activation of NFκ-B in respiratory epithelial cells [57].

In our studies, we found that EV_{ARDS} carry two Runx1 isoforms, p52 and p66. As shown in Table 3, the high ratio Runx1p66/p52 was associated with increased survival (likelihood ratio 5.218). Age, sex, SAPS II, APACHE II, SOFA, LIS, P/F ratio at the onset of ARDS or ICU length of stay cannot explain the difference. Patients with Runx1p66 isoform and a high ratio p66/p52 in their EV_{ARDS} seemed to have a higher survival as compared to patients who did not. Through this observation, it is possible that we can use the expression pattern of Runx1 isoforms as a reliable circulatory biomarker of ARDS activity.

Interestingly, our observation that EV_{ARDS}Runx1p66 might be needed only when the endogenous MSCs and lung ability to repair are not sufficient, suggests that in some long-term survivors lung resident stem cells may be involved in achieving the epithelial repair in ARDS. In fact, limited studies reported the presence of a specialized lung resident stem cell niche where type II pneumocytes function hand-in-hand with the mesenchymal stromal cells to achieve the epithelial repair following injury; it appears that the lung resident stem cell migrate from their in-tissue niche into the alveolar space and are abundant and recoverable from the bronchoalveolar lavage fluid [36].

We also observed that expression of Runx1p52 in long-term survivors gradually increases from day 1 to 37 of ICU stay (Fig. 4b). As Runx1 attenuation induces myofibroblast differentiation [34], it appears that increased expression of Runx1p52 functions to protect against excessive/pathological fibroproliferation. Thus, Runx1p52 isoform may be a novel target for therapeutic interventions to prevent pathological fibroproliferation in ARDS and a new avenue for treating severe ARDS.

Our study is first of its kind which proposes an Alk5/Runx1-mediated mechanism by which bone marrow-derived MSCs via their released EVs rescue and repair pulmonary microvascular cellular injury in ARDS. Exposure of LPS-injured human lung ECs to EV_{ARDS}Alk5Runx1p66 increases proliferation and improve junctional integrity; moreover, in LPS-treated mice, these EV_{ARDS} bearing the Runx1p66 isoform, decrease lung histological severity. By contrast, exposure to EV_{ARDS}Alk5Runx1p52 regardless of their long-term survivors or non-surviving patients source cannot induce endothelial recovery, strongly supporting the concept that Runx1p66 accounts for the beneficial effects of the EV_{ARDS}Alk5Runx1p66, and thus for the improved outcome of the long-term ARDS survivors. As the EV_{ARDS}Alk5Runx1p52 show no therapeutic benefit on LPS-treated ECs and LPS-mouse model of ALI, it appears that even if the EV_{ARDS} possess the TβR1/TβRII heteromeric complexes, the lack of the Runx1p66 isoform is critical for ARDS resolution and survival.

Though it is a robust study, we performed this translational approach in a relatively small number of ARDS patients, with a clear signal for survival in patients with EV_{ARDS}Alk5Runx1p66; however, due to small sample size and clinical heterogeneity, our finding should be confirmed in a larger cohort of patients. Our cohort included 33 ARDS patients, 29 with direct lung injury caused by pneumonia and 4 with indirect lung injury, caused by sepsis. While there may be significant overlap between direct and indirect ARDS in humans [58], the diverse treatment/medication received, concurrent illness, mechanical ventilation, use of the extracorporeal membrane oxygenation, active inflammation, etc., and the small study population without possibility of multivariable analyses may also contribute to the difference in ARDS outcome.

One other limitation of the study is the use of healthy subjects as controls. However, the contrast between the lower levels of circulating EVs in healthy conditions by comparison to disease state has been extensively reported in the literature [7, 9, 11]. Despite these limitations, this study identifies a specific subset of EV_{ARDS}Alk5Runx1p66 of MSC origin that portends a favorable prognosis for ARDS patients. Thus, Runx1p66-expressing EVs derived from MSCs cultures, have the potential of providing rapid, effective and clinically safe therapeutic approaches, and may translate into a novel 'paradigm shift' strategy to efficiently treat ARDS and promote survival. As the MSCs phenotype is different depending on the growth

stages, the observation needs to be considered when the therapeutic efficiency of the MSCs is investigated.

In sum, studies to evaluate whether or not the EV_{ARDS}Alk5Runx1p66 have a broad therapeutic effect beyond the LPS injury and to validate the finding in a larger cohort of ARDS patients will help to establish the expression pattern of Runx1 isoforms not only as a reliable circulatory biomarker of ARDS activity, but also as a novel determinant of the molecular mechanism for lung tissue repair and recovery after severe injury.

Conclusions

The expression pattern of Runx1 isoforms might be a reliable circulatory biomarker of ARDS activity and a novel determinant of the molecular mechanism for lung tissue repair and recovery after severe injury.

Additional file

Additional file 1: Table S1. Human Subjects. Detailed Clinical Data Set.

Abbreviations

ALI: acute lung injury; APACHE II: Acute Physiology and Chronic Health Evaluation II; APC: allophycocyanin; ARDS: acute respiratory distress syndrome; BCA: bicinchoninic acid; BrdU: bromodeoxyuridine; ECs: endothelial cells; EC_{LPS}: lipopolysaccharide (LPS)-treated ECs; ECMO: extracorporeal membrane oxygenation; EVs: extracellular vesicles; EV_{MSC}: mesenchymal stem cells-derived extracellular vesicles; EV_{ARDS}: extracellular vesicles isolated from the blood of ARDS patients; EV_{Ctrl}: extracellular vesicles isolated from the blood of control subjects; H&E: hematoxylin & eosin; ICU: intensive care unit; IHC: immunohistochemistry; ITSN: intersectin-1short; LIS: Lung Injury Score; LPS: lipopolysaccharide; MSCs: mesenchymal stem cells; MTT: 3-(4,5-dimethylthiazol-2-yl)-2,5-diphenyl tetrazolium bromide; ND-Ctrl: non-disease controls; TβRI: transforming growth factor receptor i; TβRII: transforming growth factor receptor ii; PBS: phosphate buffered saline; PE: phycoerythrin; P/F: PaO_2/FiO_2; RT: room temperature; RUMC: Rush University Medical Center; Runx1p52: Runx 1 p52 isoform; Runx1p66: Runx 1 p66 isoform; SAPS II: Simplified Acute Physiology Score II; SOFA: Sequential Organ Failure Assessment.

Authors' contributions

TS, DP and SP conceived and designed research; TS, SQ, CB. NJ and SdiB performed the experiments; SP, TS, MV, DP, BG, LF analyzed data; TS, DP, RB, SP interpreted results of experiments; TS, BG, SP prepared the figures; TS and SP drafted the manuscript; TS, MV and SP edited and revised the manuscript. All authors read and approved the final manuscript.

Author details

[1] Department of Internal Medicine, Pulmonary, Critical Care and Sleep Medicine, Rush University Medical Center, 1750W Harrison St. 1535 JS, Chicago, IL 60612, USA. [2] College of Nursing, Rush Medical College, Chicago, IL, USA. [3] University of Illinois at Chicago, Chicago, IL, USA. [4] Present Address: Pulmonary and Critical Care Medicine, UTSouthwestern Medical Center, Dallas, TX, USA. [5] Present Address: Pulmonary, Allergy and Critical Care Medicine, University of Alabama at Birmingham, Birmingham, AL, USA.

Acknowledgements

We would like to acknowledge Mark Maienschein-Cline, Ph.D., Director, Core for Research Informatics for data analysis and statistical support, University of Illinois at Chicago for nanoparticle analyses (NTA).

Competing interests

The authors declare that they have no competing interests.

Consent for publication

Not applicable.

Ethics approval and consent to participate

Rush University Medical Center Institutional Review Board considered that a waiver for HIPPA consent is critical for practicability in achieving high ARDS patient participation. Nevertheless, patients were told at the time of clinical consent that blood collected excess (i.e., otherwise discardable) may be used for research purposes. None of these blood samples are collected for research purposes. We have an Institutional Review Board approved protocol (IRB# 14030705-IRB01) for investigational use of un-used diseased blood samples, drawn for routine medical care that would otherwise be discarded.

All mouse studies were approved and performed in accordance with the guidelines of RUMC Institutional Animal Care and Use Committee.

Funding

This work was supported in part by National Heart, Lung, and Blood Institute, Grant R01 HL127022.

Publisher's Note

Received: 9 April 2018 Accepted: 12 June 2018
Published online: 22 June 2018

References

1. Martin TR, Matute-Bello G (2011) Experimental models and emerging hypotheses for acute lung injury. Crit Care Clin 27(3):735–752
2. Cochi SE, Kempker JA, Annangi S, Kramer MR, Martin GS (2016) Mortality trends of acute respiratory distress syndrome in the United States from 1999 to 2013. Ann Am Thorac Soc 13(10):1742–1751
3. Rubenfeld GD, Caldwell E, Peabody E, Weaver J, Martin DP, Neff M et al (2005) Incidence and outcomes of acute lung injury. N Engl J Med 353(16):1685–1693
4. Herridge MS (2011) Recovery and long-term outcome in acute respiratory distress syndrome. Crit Care Clin 27(3):685–704
5. Herridge MS, Moss M, Hough CL, Hopkins RO, Rice TW, Bienvenu OJ et al (2016) Recovery and outcomes after the acute respiratory distress syndrome (ARDS) in patients and their family caregivers. Intensive Care Med 42(5):725–738
6. Zhu YG, Feng XM, Abbott J, Fang XH, Hao Q, Monsel A et al (2014) Human mesenchymal stem cell microvesicles for treatment of *Escherichia coli* endotoxin-induced acute lung injury in mice. Stem Cells 32(1):116–125
7. Lindoso RS, Collino F, Vieyra A (2017) Extracellular vesicles as regulators of tumor fate: crosstalk among cancer stem cells, tumor cells and mesenchymal stem cells. Stem Cell Invest 4:75
8. Bern MM (2017) Extracellular vesicles: how they interact with endothelium, potentially contributing to metastatic cancer cell implants. Clin Transl Med 6(1):33
9. Peired AJ, Sisti A, Romagnani P (2016) Mesenchymal stem cell-based therapy for kidney disease: a review of clinical evidence. Stem Cells Int 2016:4798639
10. Ponte AL, Marais E, Gallay N, Langonne A, Delorme B, Herault O et al (2007) The in vitro migration capacity of human bone marrow mesenchymal stem cells: comparison of chemokine and growth factor chemotactic activities. Stem Cells 25(7):1737–1745
11. Belema-Bedada F, Uchida S, Martire A, Kostin S, Braun T (2008) Efficient homing of multipotent adult mesenchymal stem cells depends on FROUNT-mediated clustering of CCR2. Cell Stem Cell 2(6):566–575
12. Bardita C, Predescu D, Justice MJ, Petrache I, Predescu S (2013) In vivo knockdown of intersectin-1s alters endothelial cell phenotype and causes microvascular remodeling in the mouse lungs. Apoptosis 18(1):57–76
13. Force ADT, Ranieri VM, Rubenfeld GD, Thompson BT, Ferguson ND, Caldwell E et al (2012) Acute respiratory distress syndrome: the Berlin Definition. JAMA 307(23):2526–2533

14. Jeganathan N, Predescu D, Zhang J, Sha F, Bardita C, Patel M et al (2016) Rac1-mediated cytoskeleton rearrangements induced by intersectin-1s deficiency promotes lung cancer cell proliferation, migration and metastasis. Mol Cancer 15(1):59
15. Bardita C, Predescu DN, Sha F, Patel M, Balaji G, Predescu SA (2015) Endocytic deficiency induced by ITSN-1s knockdown alters the Smad2/3-Erk1/2 signaling balance downstream of Alk5. J Cell Sci 128(8):1528–1541
16. Witwer KW, Buzas EI, Bemis LT, Bora A, Lasser C, Lotvall J et al (2013) Standardization of sample collection, isolation and analysis methods in extracellular vesicle research. J Extracell Vesicles 2:20360
17. Lotvall J, Hill AF, Hochberg F, Buzas EI, Di Vizio D, Gardiner C et al (2014) Minimal experimental requirements for definition of extracellular vesicles and their functions: a position statement from the International Society for Extracellular Vesicles. J Extracell Vesicles 3:26913
18. Matthay MA, Zemans RL (2011) The acute respiratory distress syndrome: pathogenesis and treatment. Annu Rev Pathol 6:147–163
19. Predescu SA, Predescu DN, Timblin BK, Stan RV, Malik AB (2003) Intersectin regulates fission and internalization of caveolae in endothelial cells. Mol Biol Cell 14(12):4997–5010
20. Fang X, Abbott J, Cheng L, Colby JK, Lee JW, Levy BD et al (2015) Human mesenchymal stem (stromal) cells promote the resolution of acute lung injury in part through lipoxin A4. J Immunol 195(3):875–881
21. Occhetta P, Pigeot S, Rasponi M, Dasen B, Mehrkens A, Ullrich T et al (2018) Developmentally inspired programming of adult human mesenchymal stromal cells toward stable chondrogenesis. Proc Natl Acad Sci USA 115(18):4625–4630
22. Kowal J, Arras G, Colombo M, Jouve M, Morath JP, Primdal-Bengtson B et al (2016) Proteomic comparison defines novel markers to characterize heterogeneous populations of extracellular vesicle subtypes. Proc Natl Acad Sci USA 113(8):E968–E977
23. Patel M, Predescu D, Bardita C, Chen J, Jeganathan N, Pritchard M et al (2017) Modulation of intersectin-1s lung expression induces obliterative remodeling and severe plexiform arteriopathy in the murine pulmonary vascular bed. Am J Pathol 187(3):528–542
24. Patel M, Predescu D, Tandon R, Bardita C, Pogoriler J, Bhorade S et al (2013) A novel p38 mitogen-activated protein kinase/Elk-1 transcription factor-dependent molecular mechanism underlying abnormal endothelial cell proliferation in plexogenic pulmonary arterial hypertension. J Biol Chem 288(36):25701–25716
25. Enjeti AK, Ariyarajah A, D'Crus A, Seldon M, Lincz LF (2016) Correlative analysis of nanoparticle tracking, flow cytometric and functional measurements for circulating microvesicles in normal subjects. Thromb Res 145:18–23
26. Nguyen DC, Lewis HC, Joyner C, Warren V, Xiao H, Kissick HT et al (2018) Extracellular vesicles from bone marrow-derived mesenchymal stromal cells support ex vivo survival of human antibody secreting cells. J Extracell Vesicles 7(1):1463778
27. Gardiner C, Ferreira YJ, Dragovic RA, Redman CW, Sargent IL (2013) Extracellular vesicle sizing and enumeration by nanoparticle tracking analysis. J Extracell Vesicles 2:19671
28. Cohen J (1988) Statistical power analysis for the behavioral sciences. In: Erlbaum L (ed), 2nd edn. Academic Press, Hillsdale
29. Gil J (1982) Alveolar wall relations. Ann N Y Acad Sci 384:31–43
30. Lacroix R, Judicone C, Mooberry M, Boucekine M, Key NS, Dignat-George F et al (2013) Standardization of pre-analytical variables in plasma microparticle determination: results of the International Society on Thrombosis and Haemostasis SSC Collaborative workshop. J Thromb Haemost 11:1190–1193
31. Kanada M, Bachmann MH, Hardy JW, Frimannson DO, Bronsart L, Wang A et al (2015) Differential fates of biomolecules delivered to target cells via extracellular vesicles. Proc Natl Acad Sci USA 112(12):E1433–E1442
32. Chen J, Li C, Chen L (2015) The role of microvesicles derived from mesenchymal stem cells in lung diseases. Biomed Res Int 2015:985814
33. Morel O, Toti F, Hugel B, Bakouboula B, Camoin-Jau L, Dignat-George F et al (2006) Procoagulant microparticles: disrupting the vascular homeostasis equation? Arterioscler Thromb Vasc Biol 26(12):2594–2604
34. Kim W, Barron DA, San Martin R, Chan KS, Tran LL, Yang F et al (2014) RUNX1 is essential for mesenchymal stem cell proliferation and myofibroblast differentiation. Proc Natl Acad Sci USA 111(46):16389–16394
35. Tanaka T, Kurokawa M, Ueki K, Tanaka K, Imai Y, Mitani K et al (1996) The extracellular signal-regulated kinase pathway phosphorylates AML1, an acute myeloid leukemia gene product, and potentially regulates its transactivation ability. Mol Cell Biol 16(7):3967–3979
36. Sinclair KA, Yerkovich ST, Chen T, McQualter JL, Hopkins PM, Wells CA et al (2016) Mesenchymal stromal cells are readily recoverable from lung tissue, but not the alveolar space, in healthy humans. Stem Cells 34(10):2548–2558
37. Barkauskas CE, Cronce MJ, Rackley CR, Bowie EJ, Keene DR, Stripp BR et al (2013) Type 2 alveolar cells are stem cells in adult lung. J Clin Invest 123(7):3025–3036
38. Hall JB, Kress JP (2011) The burden of functional recovery from ARDS. N Engl J Med 364(14):1358–1359
39. Rich JT, Neely JG, Paniello RC, Voelker CC, Nussenbaum B, Wang EW (2010) A practical guide to understanding Kaplan–Meier curves. Otolaryngol Head Neck Surg 143(3):331–336
40. Wu C, Evans CE, Dai Z, Huang X, Zhang X, Jin H et al (2017) Lipopolysaccharide-induced endotoxemia in corn oil-preloaded mice causes an extended course of lung injury and repair and pulmonary fibrosis: a translational mouse model of acute respiratory distress syndrome. PLoS ONE 12(3):e0174327
41. Guervilly C, Lacroix R, Forel JM, Roch A, Camoin-Jau L, Papazian L et al (2011) High levels of circulating leukocyte microparticles are associated with better outcome in acute respiratory distress syndrome. Crit Care 15(1):R31
42. Shaver CM, Woods J, Clune JK, Grove BS, Wickersham NE, McNeil JB et al (2017) Circulating microparticle levels are reduced in patients with ARDS. Crit Care 21(1):120
43. Martinez M, Hinojosa M, Trombly D, Morin V, Stein J, Stein G et al (2016) Transcriptional auto-regulation of RUNX1 P1 promoter. PLoS ONE 11(2):e0149119
44. Gupta N, Su X, Popov B, Lee JW, Serikov V, Matthay MA (2007) Intrapulmonary delivery of bone marrow-derived mesenchymal stem cells improves survival and attenuates endotoxin-induced acute lung injury in mice. J Immunol 179(3):1855–1863
45. Lahm T, Crisostomo PR, Markel TA, Wang M, Lillemoe KD, Meldrum DR (2007) The critical role of vascular endothelial growth factor in pulmonary vascular remodeling after lung injury. Shock 28(1):4–14
46. Yamada M, Kubo H, Kobayashi S, Ishizawa K, Numasaki M, Ueda S et al (2004) Bone marrow-derived progenitor cells are important for lung repair after lipopolysaccharide-induced lung injury. J Immunol 172(2):1266–1272
47. Krasnodembskaya A, Song Y, Fang X, Gupta N, Serikov V, Lee JW et al (2010) Antibacterial effect of human mesenchymal stem cells is mediated in part from secretion of the antimicrobial peptide LL-37. Stem Cells 28(12):2229–2238
48. Gotts JE, Matthay MA (2011) Mesenchymal stem cells and acute lung injury. Crit Care Clin 27(3):719–733
49. Monsel A, Zhu YG, Gennai S, Hao Q, Hu S, Rouby JJ et al (2015) Therapeutic effects of human mesenchymal stem cell-derived microvesicles in severe pneumonia in mice. Am J Respir Crit Care Med 192(3):324–336
50. Armstrong SM, Wang C, Tigdi J, Si X, Dumpit C, Charles S et al (2012) Influenza infects lung microvascular endothelium leading to microvascular leak: role of apoptosis and claudin-5. PLoS ONE 7(10):e47323
51. David S, Ghosh CC, Kumpers P, Shushakova N, Van Slyke P, Khankin EV et al (2011) Effects of a synthetic PEG-ylated Tie-2 agonist peptide on endotoxemic lung injury and mortality. Am J Physiol Lung Cell Mol Physiol 300(6):L851–L862
52. Lebrin F, Deckers M, Bertolino P, Ten Dijke P (2005) TGF-beta receptor function in the endothelium. Cardiovasc Res 65(3):599–608
53. Shah TG, Bardita C, Jeganathan N, Balk RA, Predescu DN, Predescu SA (2016) Circulatory microparticles and lung endothelial cell function in acute respiratory distress syndrome patients. Am J Respir Crit Care Med 193:A5671
54. Zhang L, Fried FB, Guo H, Friedman AD (2008) Cyclin-dependent kinase phosphorylation of RUNX1/AML1 on 3 sites increases transactivation potency and stimulates cell proliferation. Blood 111(3):1193–1200
55. Iwatsuki K, Tanaka K, Kaneko T, Kazama R, Okamoto S, Nakayama Y et al (2005) Runx1 promotes angiogenesis by downregulation of insulin-like growth factor-binding protein-3. Oncogene 24(7):1129–1137
56. Friedman AD (2009) Cell cycle and developmental control of hematopoiesis by Runx1. J Cell Physiol 219(3):520–524

57. Tang X, Sun L, Jin X, Chen Y, Zhu H, Liang Y et al (2017) Runt-related transcription factor 1 regulates LPS-induced acute lung injury via NF-kappaB signaling. Am J Respir Cell Mol Biol 57:174–183
58. Shaver CM, Bastarache JA (2014) Clinical and biological heterogeneity in acute respiratory distress syndrome: direct versus indirect lung injury. Clin Chest Med 35(4):639–653
59. Garcia BA, Smalley DM, Cho H, Shabanowitz J, Ley K, Hunt DF (2005) The platelet microparticle proteome. J Proteome Res 4(5):1516–1521
60. Leroyer AS, Rautou PE, Silvestre JS, Castier Y, Leseche G, Devue C et al (2008) CD40 ligand+ microparticles from human atherosclerotic plaques stimulate endothelial proliferation and angiogenesis a potential mechanism for intraplaque neovascularization. J Am Coll Cardiol 52(16):1302–1311
61. Vasina EM, Cauwenberghs S, Feijge MA, Heemskerk JW, Weber C, Koenen RR (2011) Microparticles from apoptotic platelets promote resident macrophage differentiation. Cell Death Dis 2:e211
62. Mause SF, Ritzel E, Liehn EA, Hristov M, Bidzhekov K, Muller-Newen G et al (2010) Platelet microparticles enhance the vasoregenerative potential of angiogenic early outgrowth cells after vascular injury. Circulation 122(5):495–506
63. Mause SF, Weber C (2010) Microparticles: protagonists of a novel communication network for intercellular information exchange. Circ Res 107(9):1047–1057